



# The Benefit of a Multi-wedge Acoustic Black Hole at Low-frequency Mitigation

Max Käfer<sup>1,2</sup> · Fadi Dohnal<sup>1,2</sup>

Received: 11 December 2023 / Revised: 11 December 2023 / Accepted: 23 January 2024  
© The Author(s) 2024

## Abstract

**Introduction** Acoustic black holes (ABH) are capable to mitigate structural vibrations efficiently above a certain cut-on frequency. The most commonly used geometry for a flexible beam is a simple wedge following a power-law curve. A simple wedge demands large dimensions for achieving mitigation in the low-frequency range below 1000 Hz. It was shown recently by experiments and numerical simulation that a multi-wedge configuration is beneficial for realizing a compact design and still showing good performance at low frequencies.

**Materials and Methods** The WKB approximation is extended for a single-wedge design. Expressions for the reflection coefficient and cut-on frequency are discussed for an arbitrary number of wedges—the suggested multi-wedge ABH.

**Results** The main benefit of the stacked multi-wedge ABH is a great improvement in performance in the low-frequency range. A numerical example highlights the successful vibration mitigation. It is shown how a multi-wedge ABH is tuned towards low-frequency in terms of cut-on frequency and reflections' coefficient. The improved performance of a multi-wedge ABH is benchmarked against the well-established simple ABH.

**Keywords** Acoustic black hole · Reflection coefficient · Cut-on frequency · WKB-approximation

## Introduction

In the field of structural vibration management, methods have been divided into two main fields: passive and active strategies [1, 2]. Passive strategies include a number of established methods such as improving the damping properties of materials, incorporating viscoelastic dampers, using friction-based dampers and joints, using a variety of vibration dampers and isolation systems. The advantages of the passive approach lie in its simplicity and cost effectiveness. System stability is inherently assured and is based on the principles of energy dissipation within the structural system. In addition, their effectiveness for known systems is usually greatest for high-frequency vibrations or in a limited

frequency range, while they often underperform for vibrations at lower frequencies [3]. Effective passive vibration damping can also be achieved by employing an acoustic black hole in different geometrical configurations [4]. The idea of tapering the end of a beam to achieve an ABH goes back to [5] where a one-dimensional wedge-shaped ABH was proposed. This pioneering work was overlooked by the practical vibration community until its potential application for vibration damping was highlighted in [6]. Since then numerous geometrical shapes of the tapering of a beam have been investigated, including a stepped wedge, a trapezoidal wedge and a spiral wedge. The concept was extended from beams to two-dimensional plates in [4, 7].

All studies so far confirm the reduction in structural vibrations using this concept. Apart from the parameters describing the shape of the wedge and its material properties that define the natural frequency, the tip thickness and the damping layer are the two critical parameters to be selected for a proper design. The wedge of the tapered end follows a power law curve with a certain exponent. Theoretically, the wave speed of an incident structural plane wave tends towards zero if the length tends to infinity and the thickness of the wedge becomes zero [5]. In practise, it is impossible

✉ Max Käfer  
max.kaefer@fhv.at

<sup>1</sup> Research Center for Microtechnology, Vorarlberg University of Applied Sciences, Hochschulstraße 1, Dornbirn 6850, Vorarlberg, Austria

<sup>2</sup> Institute of Measurement and Sensor Technology, UMIT Tirol, Eduard-Wallnöfer-Zentrum 1, Hall in Tirol 6060, Tyrol, Austria

to manufacture an infinitely long wedge or a perfectly sharp tip. Therefore, the power law curve has to consider a finite tip thickness of the wedge for a realistic prediction.

For a practical size of an ABH, the vibration mitigation starts with the so-called cut-on frequency [4, 8]. Its performance below this frequency is poor. Adapting the geometry to low frequencies (< 1 kHz) or very low frequencies (< 200 Hz) demands a very long design which is unfeasible for practical applications and manufacturing. The proposed wedge design in this work achieves a reduction in cut-on frequency while keeping the dimensions of the ABH small. The effectiveness of this design was proven experimentally and calculated numerically [9]. In this work we derive analytical approximations of the reflection coefficient and the cut-on frequency for multi-wedge ABH by extending the existing WKB-approximation for a single-wedge design to the proposed design. A low reflection coefficient underlines a high-performing ABH, leading to a low amount of vibrational energy to be reflected back into the host structure to which the ABH is attached to [10, 11]. The frequency-dependent reflection coefficient is analyzed for different exponents of the power law curve and different numbers of stacked wedges. In addition, the cut-on frequency of the multi-stack design is benchmarked against an equivalent single-wedge design. It is highlighted how a multi-wedge ABH is tuned towards achieving a low reflection coefficient and low cut-on frequency that are not reachable by a single wedge of the same characteristic geometry.

### Theoretical Investigation of Wedge-Shaped Acoustic Black Holes

We start with the basic idea of the wedge-shaped acoustic black holes in [5]. Therein the wedge follows a power law curve  $h(x) = \epsilon x^m$ . If  $m \geq 2$ , the incoming wave cannot escape, if the wedge is infinitely long and its thickness decreases to zero. Figure 1 displays a schematic representation of a simple ABH. In reality the thickness  $h(x)$  cannot reach zero. Therefore, the residual thickness  $h_{tip}$  is added to the power law resulting in Eq. (1). Depending on the direction of the incoming wave, the power law curve can be written as

$$h_-(x) = (h_{tot} - h_{tip}) \left( \frac{x}{l_{abh}} \right)^m + h_{tip}, \tag{1}$$

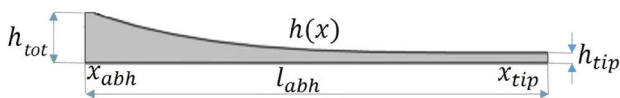


Fig. 1 Schematic representation of a simple 1D ABH based on [5]

$$h_+(x) = (h_{tot} - h_{tip}) \left( 1 - \frac{x}{l_{abh}} \right)^m + h_{tip}. \tag{2}$$

For a simple one-dimensional wedge-shaped ABH, the group and phase-velocity can be described as [6]

$$c_p = \sqrt[4]{\frac{Eh^2(x)\omega^2}{3\rho(1-\nu^2)}}, \quad c_g = \sqrt{2}c_p, \tag{3}$$

with the Young’s modulus  $E$ , the Poisson ratio  $\nu$ , the mass density  $\rho$ , the varying thickness of the wedge  $h(x)$  and the angular frequency of the bending wave  $\omega$ . For  $h_{tip} = 0$  and  $x_{tip} \rightarrow \infty$ , the phase and group velocities become zero [6, 11, 12]. The propagation time  $T_0$  from the start of the wedge at  $x_{abh}$  to its end at  $x_{tip}$  yields

$$T_0 = \int_{x_{abh}}^{x_{tip}} \frac{dx}{c_g} = \sqrt[4]{\frac{12\rho(1-\nu^2)}{E\omega^2} \frac{x_{abh}^{1-m/2} - l_{abh}^{1-m/2}}{2-m}}. \tag{4}$$

### Reflection Coefficient

For an infinitely long wedge,  $l_{abh} \rightarrow \infty$  and a sharp end,  $h_{tip} = 0$ , the propagation time in Eq. (4) becomes infinite,  $T_0 \rightarrow \infty$ , if and only if  $m \geq 2$ , as already outlined in [5]. In other words, the incident wave does not return because it is not reflected. Equations (3) and (4) show that the wedge reduces the wave velocity, which also results in the vibration energy being concentrated at the ABH, again for  $m \geq 2$ .

If the structure has a loss factor  $\eta \neq 0$ , the reflection coefficient and wavenumber is given explicitly by [10, 11, 13]

$$R = \exp \left( -2 \int_{x_{abh}}^{x_{tip}} \Im \{k(x)\} dx \right) \tag{5}$$

with

$$k(x) = \sqrt[4]{\frac{12\rho(1-\nu^2)\omega^2}{Eh^2(x)}}. \tag{6}$$

Equations (5) and (6) show that for  $x_{tip} \rightarrow \infty$  and  $h_{tip} = 0$ , the wavenumber  $k(x)$  in the ABH region tends to infinity and the reflection coefficient vanishes. This means that no wave can escape from the ABH region [11, 14]. If the ABH is partially covered with a damping layer, the reflection coefficient at any point in the damping region can be represented as a function of the thickness as [11]

$$R_0^d(x) = \left( \sqrt{\frac{\epsilon x^m}{h_{tip}}} + \sqrt{\frac{\epsilon x^m}{h_{tip}} + 1} \right)^{-K} \exp \left\{ -\frac{K_2 \eta}{2} \frac{\sqrt{\frac{\epsilon x^m}{h_{tip}}}}{\sqrt{\frac{\epsilon x^m}{h_{tip}} + 1}} \right\}, \tag{7}$$

with

$$K_2 = \frac{3v\delta}{4h_1} \frac{E_2}{E_1} \frac{\delta}{h_{tip}} K, \quad K = \sqrt[4]{\frac{12k_p^2}{\epsilon^2}}. \tag{8}$$

Herein  $v$  represents the loss factor of the absorbing layer material and  $\eta$  the loss factor of the wedge material. The layer thickness of the damping material is denoted as  $\delta$ .  $E_2/E_1$  is the ratio of the elastic moduli of the absorbing layer and the plate. The wavenumber  $k_p$  is given by the quasi-longitudinal wave velocity  $c_p$  and the angular frequency  $\omega$ , where  $k_p = \omega/c_p$ . Here,  $c_p = 2c_t(1 - c_t^2/c_l^2)^{1/2}$  holds. The longitudinal and transversal wave velocities are marked as  $c_l$  and  $c_t$ , respectively. The additional loss factor  $\xi$  can be calculated for a plate with constant thickness  $h_0$  in [10] by [15–17] as

$$\xi = \frac{v}{1 + \frac{1}{\alpha_2\beta_2(\alpha_2^2 + 3(1 + \alpha_2)^2)}}, \tag{9}$$

where  $\alpha_2$  abbreviates the ratio  $\delta/h_0$ ,  $\beta_2$  represents the ratio of the elastic moduli  $E_2/E_1$ . If the plate is covered with a damping layer on both sides, the limiting case  $\alpha_2 = \delta/h_0 \ll 1$  occurs and  $\alpha_2\beta_2 \ll 1$  must hold. Thus, Eq. (9) can be rewritten as [10]

$$\xi = 6\alpha_2\beta_2v = 6\frac{\delta}{h_0} \frac{E_2}{E_1} v. \tag{10}$$

Due to the effects and influences of a thin damping layer, the imaginary part of the wave number can be calculated as a function of local thickness  $h(x)$  as

$$\Im\{k(x)\} = \sqrt[4]{\frac{12k_p^2}{h^2(x)} \left[ \frac{v}{4} + \frac{3}{2} \frac{\delta}{h(x)} \frac{E_2}{E_1} v \right]}. \tag{11}$$

For a quadratic wedge of the form  $h(x) = \epsilon x^2 + h_{tip}$ , an analytic solution for the reflection coefficient  $R_0$  can be found by substituting Eq. (11) into Eq. (5) [10].

$$R_0^{(m=2)} = \exp(-2\mu_1^{(m=2)} - 2\mu_2^{(m=2)}) \tag{12}$$

with

$$\mu_1^{(m=2)} = \sqrt[4]{\frac{12k_p}{\epsilon^2} \frac{\eta}{4} \ln \frac{x}{x_{tip}}} \tag{13}$$

and

$$\mu_2^{(2)} = \sqrt[4]{\frac{12k_p}{\epsilon^6} \frac{3v\delta}{4} \frac{E_2}{E_1} \left( \frac{1}{x_{tip}^2} - \frac{1}{x^2} \right)}. \tag{14}$$

Compared to the reflection coefficient in Eq. (7), no explicit value for the height  $h_{tip}$  of the wedge occurs. The dependence here is implicitly given by the total length  $l_{abh}$  and its intercept at the point  $x_{tip}$ . The dependence of the reflection coefficient on the tip height  $h_{tip}$  is exploited for practical manufacturing. In [10, 11], an equivalent theoretical solution was found by expressing the dependency in terms of  $x_{abh}$ .

Repeating the calculation above for  $m = 4$  starting from Eq. (5), i.e.  $h(x) = \epsilon x^4 + h_{tip}$ , the following reflection coefficient is derived [10]

$$R_0^{(m=4)} = \exp\left(-2\mu_1^{(m=4)} - 2\mu_2^{(m=4)}\right) \tag{15}$$

with

$$\mu_1^{(m=4)} = \sqrt[4]{\frac{12k_p}{\epsilon^2} \frac{\eta}{4} \left[ \frac{1}{x_{tip}} - \frac{1}{x} \right]} \tag{16}$$

and

$$\mu_2^{(m=4)} = \sqrt[4]{\frac{12k_p}{\epsilon^6} \frac{3v\delta}{10} \frac{E_2}{E_1} \left[ \frac{1}{x_{tip}^5} - \frac{1}{x^5} \right]}. \tag{17}$$

Expressions for other values of  $m$  can be found in [18].

If no damping layer is present then  $\delta=0$  and  $v=0$  and the exponents  $\mu_2^{(m=2)} = 0$  and  $\mu_2^{(m=4)} = 0$  as outlined in [10]. The reflection coefficient  $R_0$  defined in Eqs. (12) and (15) for these two cases is visualised in Fig. 2 in dependency of the length of a simple-wedge satisfying the power law curve  $h(x) = \epsilon x^m$ . The remaining system parameters chosen are listed in Table 1 in for a simple-wedge ABH. It can be clearly seen that the increase of the exponent  $m$  leads to a lower value of reflection coefficient which means that less kinetic energy from the incident wave is reflected from the ABH back into the host structure. Increasing the exponent from its minimum value  $m = 2$  to  $m = 4$  results already in a significant decrease of  $R_0$ .

Stacking a number of  $n$  wedges stacked on top of each other yields a multi-wedge ABH as sketched schematically in Fig. 3. Note that the total height  $h_{tot}$  remains constant for a fair comparison of the mitigation performance between a multi-wedge and a single-wedge ABH.

For the calculation of the reflection coefficient  $R_0$  without damping layer for a multi-wedge ABH, the schematic representation in Fig. 4 is used. The shear force of the incoming plane bending wave is split to shear forces acting on the individual wedge within the cross-section between the host structure and the two-wedge ABH,  $F = F_1 + F_2$ . With the width  $b$  and the individual heights  $h_1$  and  $h_2$  for the

comparison powerlaw – curve  $m = 2$  and  $m = 4$

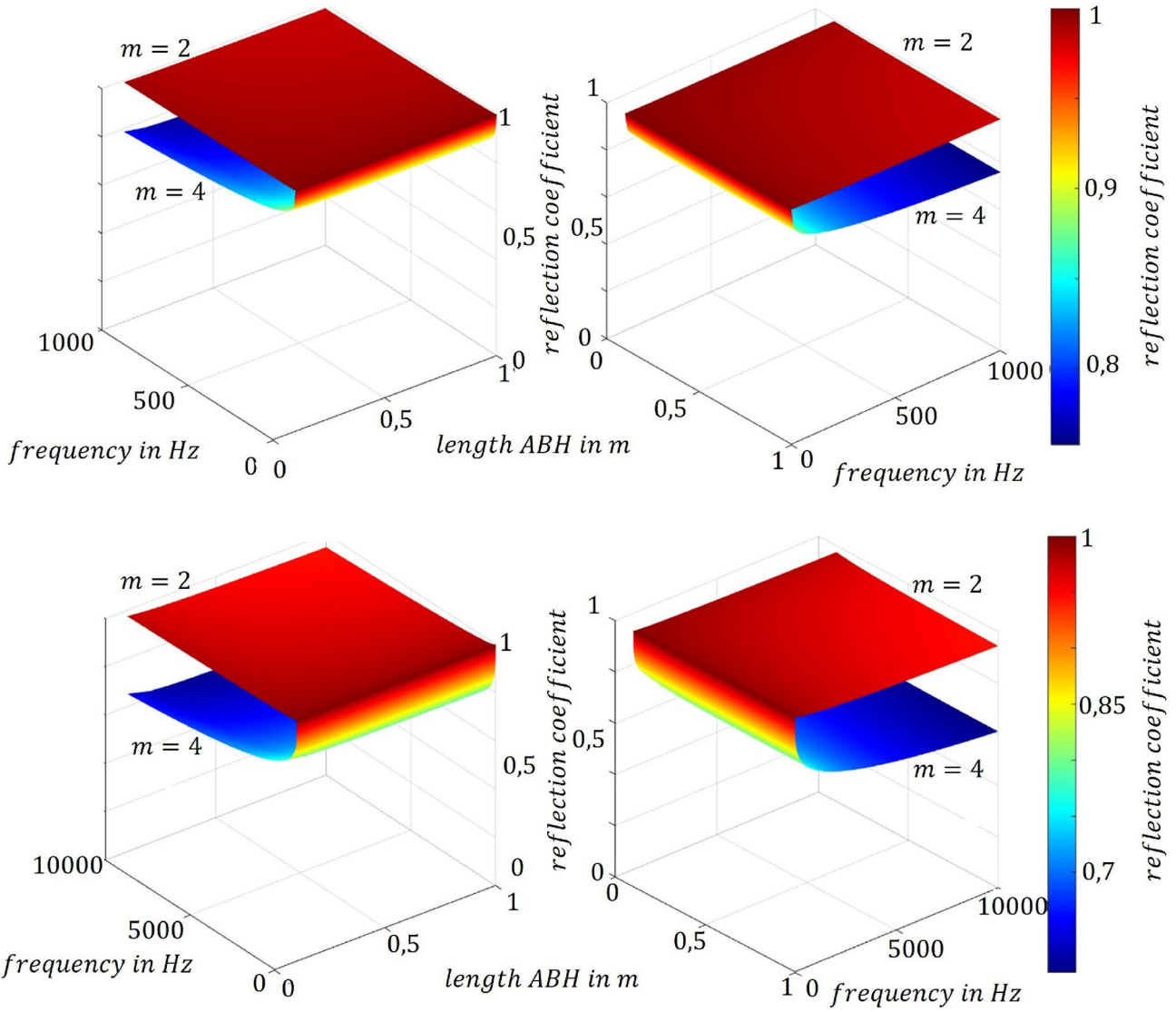


Fig. 2 Comparison of reflection coefficients (Eqs. (12), (15)) for ( $h_{tip} \ll 0, 1$  mm) with  $m = 2$  and  $m = 4$  and without damping layer. (top): low-frequency range up to 1000 Hz, (bottom): high-frequency range up to 10000 Hz

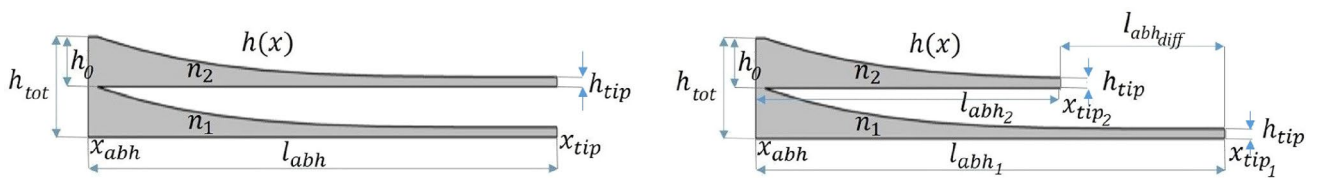


Fig. 3 Schematic representation of a multi-wedge ABH introduced in [9] for the same and for different wedge lengths

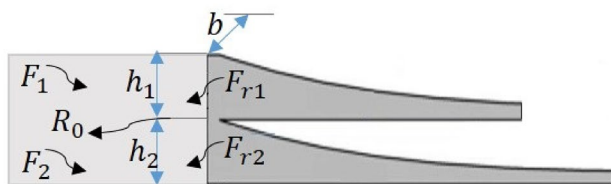


Fig. 4 Multi-wedge 1D ABH with reflection coefficient  $R_0$

two-wedge ABH in Fig. 4, this relation can be reformulated to  $p_{in}b(h_1 + h_2) = p_{in}bh_1 + p_{in}bh_2$ , where  $p_{in}$  is the surface force of the incident wave acting on the cross-section. Consequently, the reflection coefficient between the incoming and reflected wave of a two-wedge becomes

$$R_{tot}^{(n=2)} = \frac{R_1 p_{in} b h_1 + R_2 p_{in} b h_2}{p_{in} b (h_1 + h_2)} = \frac{R_1 h_1 + R_2 h_2}{h_{tot}} \tag{18}$$

For the special case of a two-wedge with identical wedge heights  $h_1 = h_2$ , the individual reflection coefficients are identical,  $R_1 = R_2$ , and the total reflection coefficient becomes  $R_{tot} = R_1$ . For an arbitrary number  $n$  of the wedges, the total reflection coefficient reads

$$R_{tot}^{(n)} = \frac{\sum R_n h_n}{h_{tot}} \quad \text{where} \quad h_{tot} = \sum_n h_n \tag{19}$$

Introducing multiple wedges leads to an additional and significant decrease of the reflection coefficient compared to Fig. 2. A comparison of the reflection coefficient (eq. (15)) for a simple-wedge and ten-wedge ABH for  $m = 4$  is shown in Fig. 5. The ten-wedge clearly outperforms the simple wedge configuration. In the plotted frequency range up to 10000 Hz, the reflection coefficient is reduced by 50% from 0,68 for the simple wedge down to a value of 0,29 for the ten-wedge. Note that the total height  $h_{tot}$  and the length of both configurations are identical.

Figure 6 shows the calculated reflection coefficient according to Eq. (5) starting from a simple wedge from a ten-wedge ABH up to the full ten-wedge ABH without a damping layer as function of the frequency. The physical parameters are listed in Table 1. With an increasing number  $n$  of stacked wedges the individual height of each wedge  $h_0$  as well as  $h_{tip}$  remains the same while the total height  $h_{tot}$  increases. It can be clearly seen that each additional wedge layer decreases the reflection coefficient further. The higher the number of stacked wedges the stronger the decrease becomes. Additionally, the gradients  $g_n$  were calculated.

An energy ratio between the multi-wedge and the host structure is evaluated to highlight the improved performance of stacked multi-wedges. The energy ratio is the ratio between the kinetic energy in the wedges and the kinetic energy in the host structure where the incident wave originates from. These values are calculated using a finite element model. Table 2 lists the first five natural frequencies

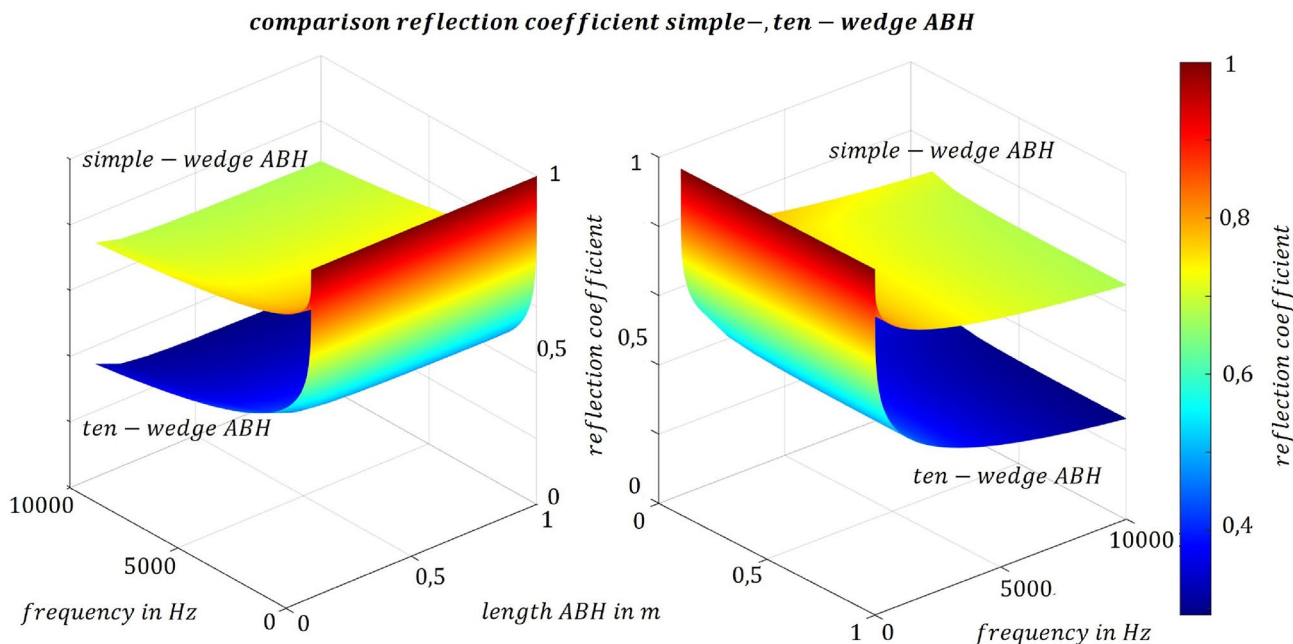


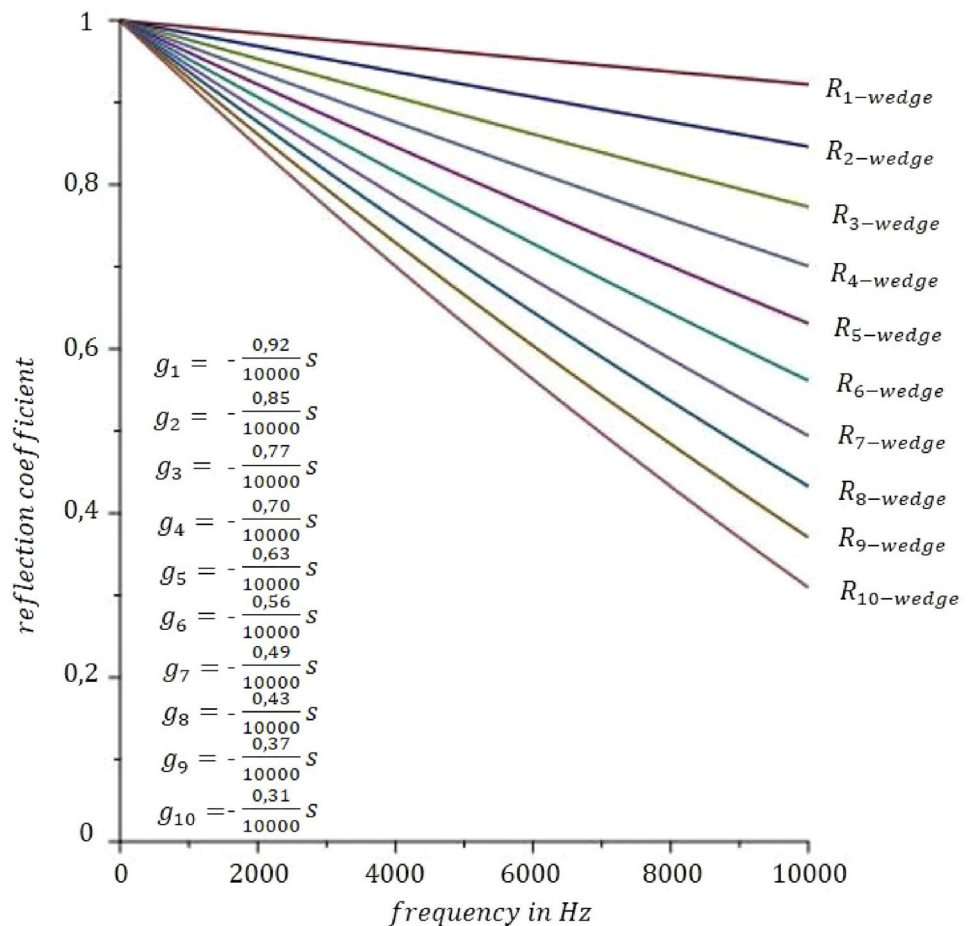
Fig. 5 Comparison of the reflection coefficients (Eq. (15)) of a simple- and ten-wedge ABH with dimensions listed in Table 1 for  $m = 4$ ,  $h_{tip} \ll 0,1 \text{ mm}$

**Table 1** Geometrical parameters for example multi-wedge ABH given in mm

$l_{abh}$	$h_{tot}$	$b$	$n$	$h_0$	$h_{tip}$	$m$	$E$	$\eta$	$\rho$	$\nu$
50	5	30	1	5	1	4	210	$10^{-3}$	7850	0,28
50	5	30	2	2,5	0,5	4	210	$10^{-3}$	7850	0,28
50	5	30	3	1,67	0,33	4	210	$10^{-3}$	7850	0,28
50	5	30	4	1,25	0,25	4	210	$10^{-3}$	7850	0,28
50	5	30	5	1,00	0,20	4	210	$10^{-3}$	7850	0,28
50	5	30	6	0,83	0,17	4	210	$10^{-3}$	7850	0,28
50	5	30	7	0,71	0,14	4	210	$10^{-3}$	7850	0,28
50	5	30	8	0,63	0,13	4	210	$10^{-3}$	7850	0,28
50	5	30	9	0,56	0,11	4	210	$10^{-3}$	7850	0,28
50	5	30	10	0,50	0,10	4	210	$10^{-3}$	7850	0,28

Number of wedges  $n$ , loss-factor  $\eta$ , Poisson's ratio  $\nu$  and exponent of the power law curve  $m$  are dimensionless.  $E$  and  $\rho$  are given in GPa and  $\text{kg/m}^3$

**Fig. 6** Reflection coefficients  $R$  (Eq. (5)) starting from a simple wedge up to a ten-wedge ABH ( $R_{1\text{-wedge}}$  to  $R_{10\text{-wedge}}$ ) and gradient listed as  $g_n$  for  $h_{tip} = 0,1 \text{ mm}$



for a simple-wedge and a ten-wedge configuration and its corresponding energy ratios for a host structure being a steel beam with a length of 250 mm, width  $b = 30 \text{ mm}$  and a total height  $h_{tot} = 5 \text{ mm}$ . The ten-wedge ABH shows significantly lower and more natural frequencies in the low-frequency range starting from 128 Hz. The energy ratio is orders of

magnitude higher for the multi-wedge. Consequently, much more energy is present in the wedges than in the host structure which underlines the lower reflection coefficient discussed in the previous paragraphs. This confirms the high performance of a multi-wedge ABH in the low-frequency range while keeping the same outer dimensions.

**Table 2** First five eigenfrequencies for simple-wedge ABH and ten-wedge ABH with energy ratios between ABH and 250 mm steel beam as base structure

EF simple-wedge ABH	energy ratio ABH/ beam simple-wedge ABH	EF ten-wedge ABH	energy ratio ABH/ beam ten-wedge ABH
501 Hz	0.56	128 Hz	519,79
967 Hz	1,67	129 Hz	226,31
1645 Hz	0,40	130 Hz	226,31
1970 Hz	3,92	131 Hz	631,71
2529 Hz	0,43	134 Hz	14,27

This idea can be extended easily to a two-dimensional ABH by performing a rotation of the one-dimensional ABH. The tip of the ABH is the located in the center [19, 20]. The theoretical analysis in case of thin plate can be found [21]. A systematic summary of the theoretical analysis including a two-dimensional ABH was performed in [22]. Placing a damping material on the in the ABH region, the structure can be considered as a composite structure. The total loss factor can be expressed as [21]

$$\eta_{comp}(r) = \frac{\eta_D \frac{E_D h_D}{E_w h(r)} \left[ 4 \left( \frac{h_D}{h(r)} \right)^2 + 6 \left( \frac{h_D}{h(r)} \right) + 3 \right]}{1 + \frac{E_D h_D}{E_w h(r)} \left[ 4 \left( \frac{h_D}{h(r)} \right)^2 + 6 \left( \frac{h_D}{h(r)} \right) + 3 \right]}, \quad (20)$$

where  $E_D$  and  $h_D$  are the modulus of elasticity and the thickness of the damping layer,  $\eta_D$  the loss factor of the damping material and  $E_w$  the Young’s modulus of the plate material.  $h(r)$  represents the thickness of the plate following the power law curve. The distance to the center of the ABH is denoted by  $r$ . As  $r$  decreases, the dissipation factor increases which means more vibration energy is absorbed. The reflection coefficient of the ABH becomes

$$R_0^{plate} = \exp \left\{ -\sqrt{\frac{12\omega^2[\rho(1-\nu^2)]}{\epsilon^2 E}} \frac{3}{4} \int_{R_i}^{R_o} \eta_{comp}(r) \frac{dr}{r} \right\}, \quad (21)$$

where  $R_o$  is the radius of the entire ABH and  $R_i$  is the section length, i.e. the radius of the inner hole [11, 21].

**WKB-Approximation**

The Wentzel-, Kramers-, Brillouin-approximation (WKB-approximation) from quantum mechanics can generate analytical solutions of various orders of approximation for differential equations [23, 24]. The WKB-approximation

normally is used to solve wave equations. Here we use it to derive an approximation of the flexural vibration and the reflection coefficient. The first WKB-approximation was derived based on the conservation of energy for eq. (22) in [24]. For higher order approximations, similar to [25], a more general approach is used here [23, 26]. For a wedge-shaped ABH with infinite width  $b$  in the  $y$ -direction, a scenario can be considered where only the system variables vary in the  $x$ -direction. One-dimensional harmonic bending waves in a thin plate with varying thickness  $h(x)$  can be described by the output equation Eq. (23) as a fourth-order differential equation [23, 26, 27]

$$[D(x)w''(x, \omega)]'' - \omega^2 \rho h(x)w(x, \omega) = 0. \quad (22)$$

Here  $w(x, \omega)$  represents the complex transverse displacement amplitude at the center of the plate,  $\omega$  the angular frequency,  $\rho$  the density from the plate material and  $D(x) = \rho c^2 h^3(x)/12$  the bending stiffness. The independent variable of the differential equation is the spatial coordinate  $x$ . The conversion for the time change of the harmonic displacement is  $e^{i\omega t}$  with imaginary unit  $i$  [23, 26]. The corresponding equation for this for bending waves in thin beams is given by [27]

$$[B(x)w''(x, \omega)]'' - \omega^2 \rho A_{QS}(x)h(x)w(x, \omega) = 0. \quad (23)$$

$B(x) = EI(x)$  represents the bending stiffness, with Young’s modulus  $E$  and moment of inertia  $I(x)$ . The cross-sectional area is denoted by  $A_{QS}(x)$ . It is  $I(x) = bh^3(x)/12$  and  $A_{QS} = bh(x)$  with the width of the beam  $b$ . If the width is constant, the preceding equation can be transformed into

$$\left[ \frac{Eh^3(x)}{12} w''(x, \omega) \right]'' - \omega^2 \rho h(x)w(x) = 0. \quad (24)$$

The WKB-method can produce the following form for the wave equation Eq. (22) by an expansion with a factor defined as  $\epsilon = \omega^{-1/2}$ .

$$\epsilon^4 (Dw'')'' - \rho h w = 0. \quad (25)$$

For the transverse displacement, according to [23, 26], a trial solution in the form of an infinite exponential series can be generated as

$$w = A e^{\epsilon^{-1} \sum_{n=0}^{\infty} S_n \epsilon^n}, \quad \epsilon \rightarrow 0. \quad (26)$$

The functions  $S_n$  change with position and frequency.  $A$  represents an arbitrary complex constant, with the dimensions of the displacement. In Eq. (26), the enhancement factor  $\epsilon$  goes to zero when the frequency goes to infinity. If The trial solution from Eq. (26) is substituted into Eq. (25) after all terms are divided by the exponent, the result can be rearranged as a polynomial equation of  $\epsilon$ . These equations must hold for all values of  $\epsilon$  so that an infinite series of differential

equations can be obtained [23, 26, 28, 29]. The first equations can be represented as follows [23]

$$\epsilon^0 : S_0' = \frac{\rho h}{D} = \frac{12}{c^2 h^2}, \tag{27}$$

$$\epsilon^1 : S_1' = -\frac{3S_0''}{2S_0'} - \frac{1D'}{2D}, \tag{28}$$

$$\epsilon^2 : S_2' = -\frac{3S_1'^2}{2S_0'} - \frac{3S_1''}{2S_0'} - 3\frac{S_0''S_1'}{S_0'^2} - \frac{S_0'''}{S_0'^2} - \frac{3S_0''^2}{4S_0'^3} - \frac{3D'S_1'}{2DS_0'} - \frac{1D''1}{4DS_0'} - \frac{3D'S_0''}{2DS_0'^2}. \tag{29}$$

According to [23, 26], the WKB-approximation can be written inferentially for a number of  $N$  approximations as

$$w = Ae^{\epsilon^{-1} \sum_{n=0}^N S_n \epsilon^n}. \tag{30}$$

whereas a generalized form for  $w(x)$  can be represented as

$$w(x) = Ae^{\frac{S_0(x) + \epsilon S_1(x) + \epsilon^2 S_2(x) + \epsilon^3 S_3(x) + \epsilon^4 S_4(x)}{\epsilon}}. \tag{31}$$

The curve from Eq. (1) and  $k(x)$  for a simple ABH can now be used to calculate the individual  $S_n$  functions which results in

$$S_0'(x) = \pm \frac{12^{\frac{1}{4}} (\rho E^3 h(x)^2)^{\frac{1}{4}}}{Eh(x)}, \quad \frac{i 12^{\frac{1}{4}} (\rho E^3 h(x)^2)^{\frac{1}{4}}}{Eh(x)}, \tag{32}$$

$$S_1'(x) = -\frac{3}{4} \frac{h'(x)}{h(x)}. \tag{33}$$

Now  $w(x)$  can be written as

$$w(x) = A \left( \frac{h(0)}{h(x)} \right)^{3/4} e^{\frac{S_0(x) + \epsilon^2 S_2(x) + \epsilon^3 S_3(x) + \epsilon^4 S_4(x)}{\epsilon}}. \tag{34}$$

Following  $S_2'(x)$  can be stated as

$$S_2'(x) = \frac{\sqrt{2} 3^{\frac{3}{4}} E \left( 28(h''(x))h(x) + 3(h'(x))^2 \right)}{192h(x)(\rho E^3 h(x)^2)^{\frac{1}{4}}}. \tag{35}$$

Due to the complexity and length of the derivatives  $S_3'(x)$  and  $S_4'(x)$ , the equations are not displayed in the manuscript but can be followed in [23, 26]. The power law curves  $h_-(x)$  and  $h_+(x)$  (Eqs. (1), (2)) can now be substituted in the equations for  $S_n'(x)$ . First  $h_-(x)$  Eq. (1) is substituted, which leads to

$$S_0'(x)_- = \frac{i 12^{\frac{1}{4}} \left( \rho E^3 \left( \frac{(h_{tot} - h_{tip})x^m}{l_{abh}^m} + h_{tip} \right)^2 \right)^{\frac{1}{4}}}{E \left( \frac{(h_{tot} - h_{tip})x^m}{l_{abh}^m} + h_{tip} \right)}, \tag{36}$$

Again, the equations for  $S_2'(x)_-$ ,  $S_3'(x)_-$  and  $S_4'(x)_-$  are too cumbersome and are not given explicitly here. Following, physical values for the ABH are inserted. The physical values for this were taken from the practical applications of this work and used for the fabricated steel ABH. A Young's modulus of  $E = 2.1 \cdot 10^{11}$  GPa, density of  $\rho = 7850$  kg/m<sup>3</sup>, height of ABH  $h_{tot} = 5$  mm, height tip of ABH  $h_{tip} = 1$  mm, length  $l_{ABH} = 50$  mm were used for calculation. Furthermore values of  $A = 1$  and  $\epsilon = \frac{\sqrt{5}}{1000\sqrt{\pi}}$ , which corresponds to 100000 Hz, were used. [23, 26] states that the WKB-approximation is only relevant for high frequencies. Following the displacement  $w(x)$  can be calculated with

$$w_0(x)_- = e^{200\sqrt{5}\sqrt{\pi} S_0(x)}, \tag{37}$$

$$w_1(x)_- = \frac{0,006e^{200\sqrt{5}\sqrt{\pi} S_0(x)}}{(640x^4 + 0,001)^{\frac{3}{4}}}, \tag{38}$$

$$w_2(x)_- = \frac{0,006e^{200\left(\frac{S_2(x)}{200000\pi} + S_0(x)\right)\sqrt{5}\sqrt{\pi}}}{(640x^4 + 0,001)^{\frac{3}{4}}}, \tag{39}$$

$$w_3(x)_- = \frac{0,006e^{200\left(\frac{\sqrt{5}S_3(x)}{200000000\pi^{\frac{3}{2}}} + \frac{S_2(x)}{200000\pi} + S_0(x)\right)\sqrt{5}\sqrt{\pi}}}{(640x^4 + 0,001)^{\frac{3}{4}}}, \tag{40}$$

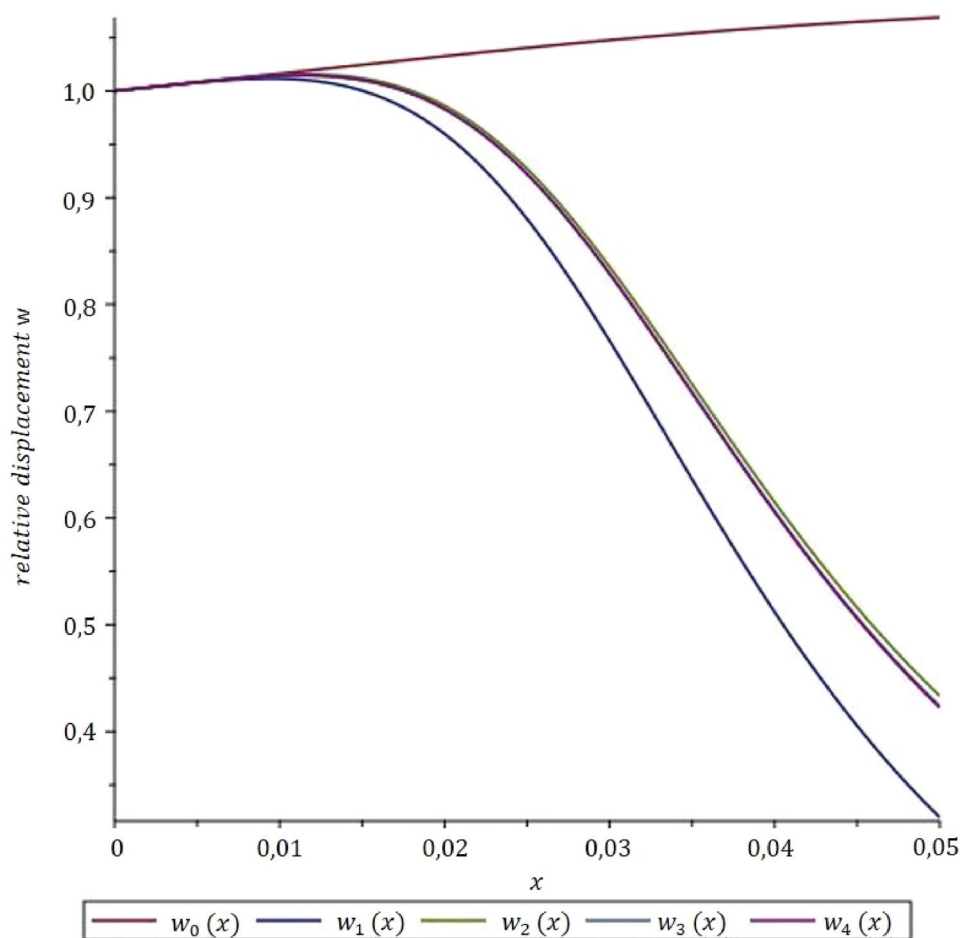
$$w_4(x)_- = \frac{0,006e^{200\left(\frac{S_4(x)}{400000000000\pi^2} + \frac{\sqrt{5}S_3(x)}{200000000\pi^{\frac{3}{2}}} + \frac{S_2(x)}{200000\pi} + S_0(x)\right)\sqrt{5}\sqrt{\pi}}}{(640x^4 + 0,001)^{\frac{3}{4}}}. \tag{41}$$

This can be plotted for the relative displacement  $w$  for a travelling wave over the length of the ABH shown in Fig. 7. It can be seen that if a wave is travelling from the tip of the ABH  $x_{tip} = 0$  to the end of the ABH  $x_{abh} = 0,05$  the relative displacement is attenuated for higher order approximations. Underlining a resting beam structure while the ABH is oscillating.

The same procedure now can be applied to the power law curve  $h_+(x)$  Eq. (2), which is substituted into  $S_n'(x)$ . This leads to



**Fig. 7** Relative displacement  $w$  for a travelling wave over the length of the ABH from  $x_{tip} = 0$  to  $x_{abh} = 0,05$



$$S'_0(x)_+ = \frac{i 12^{\frac{1}{4}} \left( \rho E^3 \left( (h_{tot} - h_{tip}) \left( 1 - \frac{x}{l_{abh}} \right)^m + h_{tip} \right)^2 \right)^{\frac{1}{4}}}{E \left( (h_{tot} - h_{tip}) \left( 1 - \frac{x}{l_{abh}} \right)^m + h_{tip} \right)} \tag{42}$$

The equations for  $S'_2(x)_+$ ,  $S'_3(x)_+$  and  $S'_4(x)_+$  are too cumbersome and are not given explicitly here. Now the physical values are inserted again. Now the displacement  $w(x)$  is given by

$$w_0(x)_+ = e^{200\sqrt{5}\sqrt{\pi}S_0(x)} \tag{43}$$

$$w_1(x)_+ = \frac{0,02e^{200\sqrt{5}\sqrt{\pi}S_0(x)}}{(0,004(1 - 20x)^4 + 0,001)^{\frac{3}{4}}} \tag{44}$$

$$w_2(x)_+ = \frac{0,02e^{200\left(\frac{S_2(x)}{2000000\pi} + S_0(x)\right)\sqrt{5}\sqrt{\pi}}}{(0,004(1 - 20x)^4 + 0,001)^{\frac{3}{4}}} \tag{45}$$

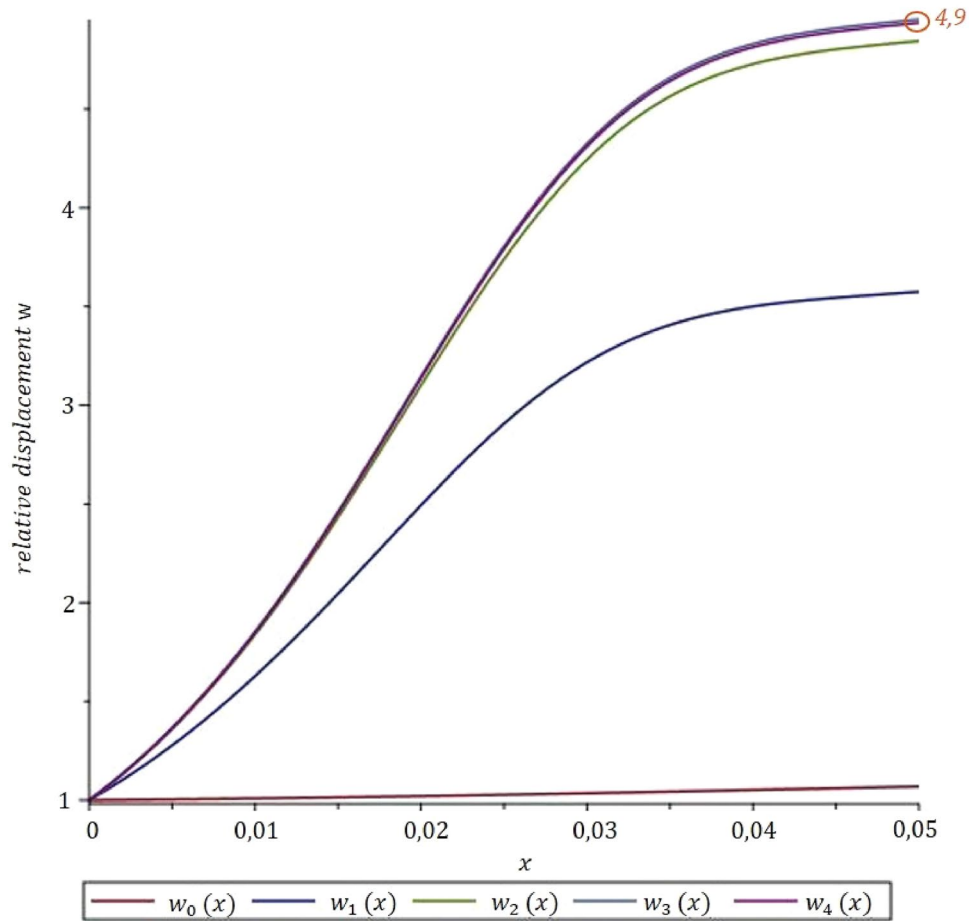
$$w_3(x)_+ = \frac{0,02e^{200\left(\frac{\sqrt{5}S_3(x)}{200000000\pi^{\frac{3}{2}}} + \frac{S_2(x)}{200000\pi} + S_0(x)\right)\sqrt{5}\sqrt{\pi}}}{(0,004(1 - 20x)^4 + 0,001)^{\frac{3}{4}}} \tag{46}$$

$$w_4(x)_+ = \frac{0,02e^{200\left(\frac{S_4(x)}{40000000000\pi^2} + \frac{\sqrt{5}S_3(x)}{200000000\pi^{\frac{3}{2}}} + \frac{S_2(x)}{200000\pi} + S_0(x)\right)\sqrt{5}\sqrt{\pi}}}{(0,004(1 - 20x)^4 + 0,001)^{\frac{3}{4}}} \tag{47}$$

This time the wave is travelling from the end of the ABH  $x_{abh} = 0$  to the tip of the ABH  $x_{tip} = 0,05$ . The relative displacement  $w$  over the length of the ABH shown in Fig. 7. It can be seen that the travelling wave from the end to the tip of the ABH is amplified for higher order approximations of the relative displacement, underlining that the tip of the ABH is oscillating while the beam at the end of the ABH is at its rest.

The relative displacement in Fig. 7 and Fig. 8 states clearly that the displacement is attenuated if travelling

**Fig. 8** Relative displacement  $w$  for a travelling wave over the length of the ABH from  $x_{abh} = 0$  to  $x_{tip} = 0,05$  with marked displacement of 4,9 of highest order approximation



from  $x_{tip}$  to  $x_{abh}$  and amplified if travelling from  $x_{abh}$  to  $x_{tip}$ . If the amplitude of relative displacement is 1 for  $w_4(x)_-$  at  $x_{tip} = 0$  it shifts to 0,42 at  $x_{abh} = 0,05$ . Vice versa if the amplitude of relative displacement is 1 for  $w_4(x)_+$  at  $x_{abh} = 0$  it shifts to 4,9 at  $x_{tip} = 0,05$ . This underlines the effectiveness of the ABH and was proven using the WKB-method for higher order approximations, stating a resting beam structure at the end of the ABH and an oscillating tip of the ABH.

A more general analytical approximation of the displacement at the tip of the ABH can be stated in the following Eq. (48). In this case approximations of the  $S_n(x = x_{tip})$  values calculated with the leading term in each Taylor series were used.

$$w(l_{abh}) \approx A \left( \frac{h_{tot}}{h_{tip}} \right)^{\frac{3}{4}} e^{\frac{7mcE^{\frac{3}{4}}(h_{tot}-h_{tip})\sqrt{2}}{48l_{abh}(\rho E^3 h_{tip}^2)^{\frac{1}{4}}}} \tag{48}$$

If the physical values are substituted into Eq. (48) an amplitude of displacement of 5,1 can be calculated. Compared

to the amplitude of displacement calculated numerical for  $w_4(x)_+$  of 4,9 at  $x_{tip} = 0,05$  a difference of 4% can be presented. Like stated in [23, 26] the approximation only applies to the higher frequency range.

### Cut-On Frequency

The cut-on frequency for an acoustic black hole serves as the cut-on frequency above which sound energy can be effectively absorbed. This frequency functions similarly to the event horizon of a conventional black hole in that it represents the point at which it achieves its intended effect. Conversely, below the cut-on frequency, wave absorption cannot occur because the wavelength of the incoming wave is greater than the physical length of the ABH [4, 8]. From [8], the derivation of the cut-on frequency can be obtained analytically, of the form Eq. (49) [4]. The solution approach for an ABH with a power law curve of the form  $h(x) = \epsilon x^m$  can be solved analytically to some extent via the wave equation for one-dimensional waves in solids and the harmonic solution. Since in [8] certain equation terms are omitted.

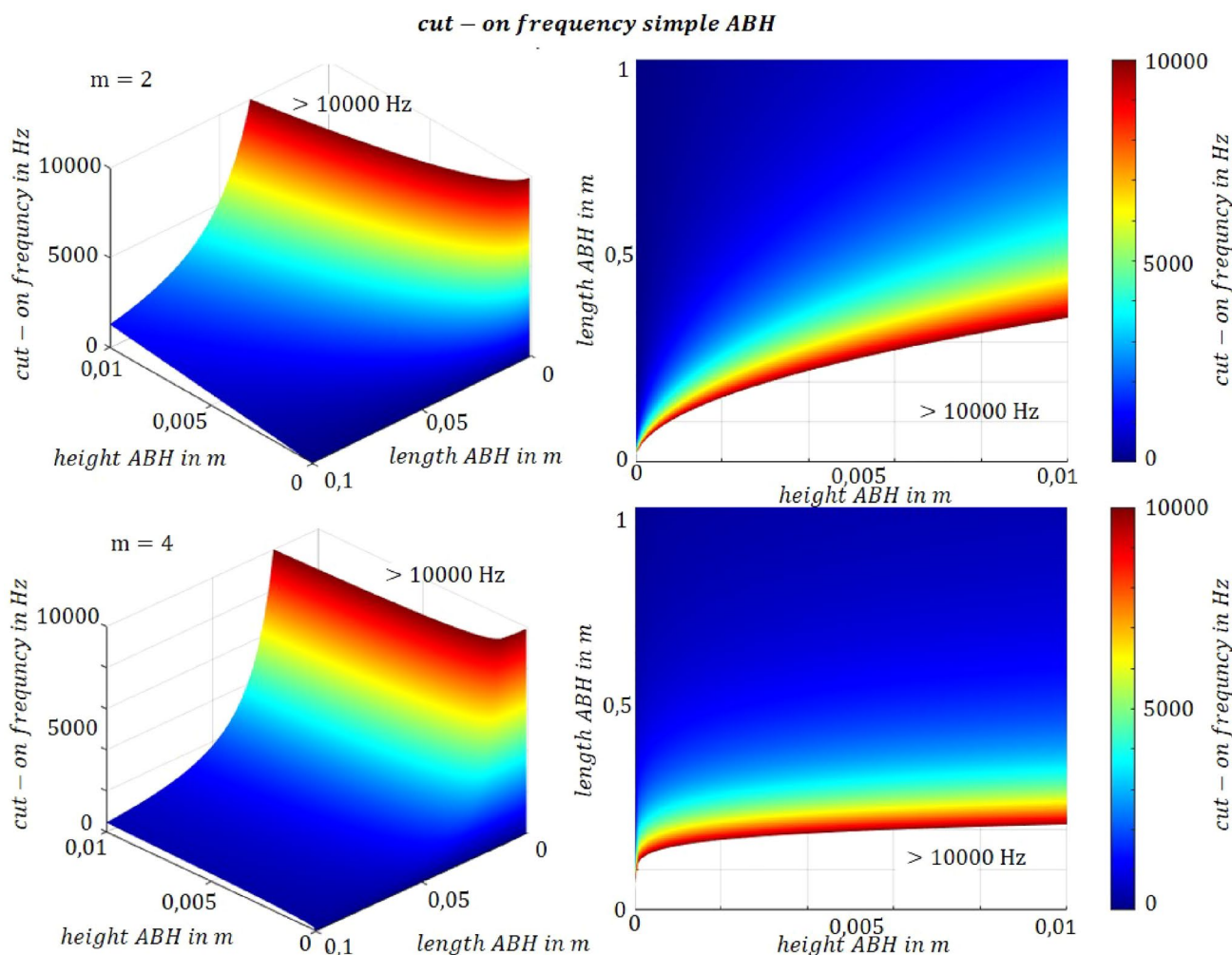


**Fig. 9** Cut-on frequency for a simple ABH with (top):  $m=2$  and (bottom):  $m=4$

Figure 9 shows the cut-on frequency for the cases  $m=2$  (top) and  $m=4$  (bottom) as a function of the structure height and length of the ABH.  $h(x) = \epsilon x^4$  shows lower cut-on frequencies for lower ABH lengths. This confirms, that its possible to achieve the same cut-on frequency with a much shorter ABH if the power law curve with  $m=4$  is used. For practical applications this could result in a smaller amount of material, which is used to manufacture the ABH. For a additional comparison between a simple-wedge ABH and ten-wedge ABH with  $l_{abh}=50$  mm,  $m=4$  the energy was calculated for both as function of frequency in Fig. 10 with a loss-factor  $\eta = 10^{-3}$  and  $\eta = 2 \cdot 10^{-3}$ . Each peak in the figure marks an eigenfrequency. The dashed lines are marking the cut-on frequency for each configuration. It is clearly to be seen, that the stacked ten-wedge ABH has a significantly lower cut-on frequency at 128 Hz, allowing it to absorb vibrational

energy in much lower frequency ranges. The pointed lines are showing the energy for both the simple-wedge ABH and ten-wedge ABH with  $\eta = 2 \cdot 10^{-3}$ . It can be seen that an increasing  $\eta$  lowers the energy in the wedges of the ABH. The cut-on frequency for the simple-wedge ABH is marked at 501 Hz. Furthermore the stacked ABH has much more eigenfrequencies lower than 1500 Hz.

$$f_{cut-on}(m) = \frac{h_{tot}^{1/m}}{2\pi l_{abh}^2} \sqrt[m]{\frac{E(40 - 24\nu)}{12\rho(1 - \nu^2)}} \tag{49}$$

In addition the reflection coefficient (Eq. (15)) for a simple- and ten-wedge ABH was displayed in Fig. 11 up to 1500 Hz with different loss-factors. It can be seen that

**Fig. 10** Energy for a simple-wedge ABH and ten-wedge ABH with  $l_{abh}=50$  mm for  $m=4$  and marked cut-on frequency with different loss-factors  $\eta$

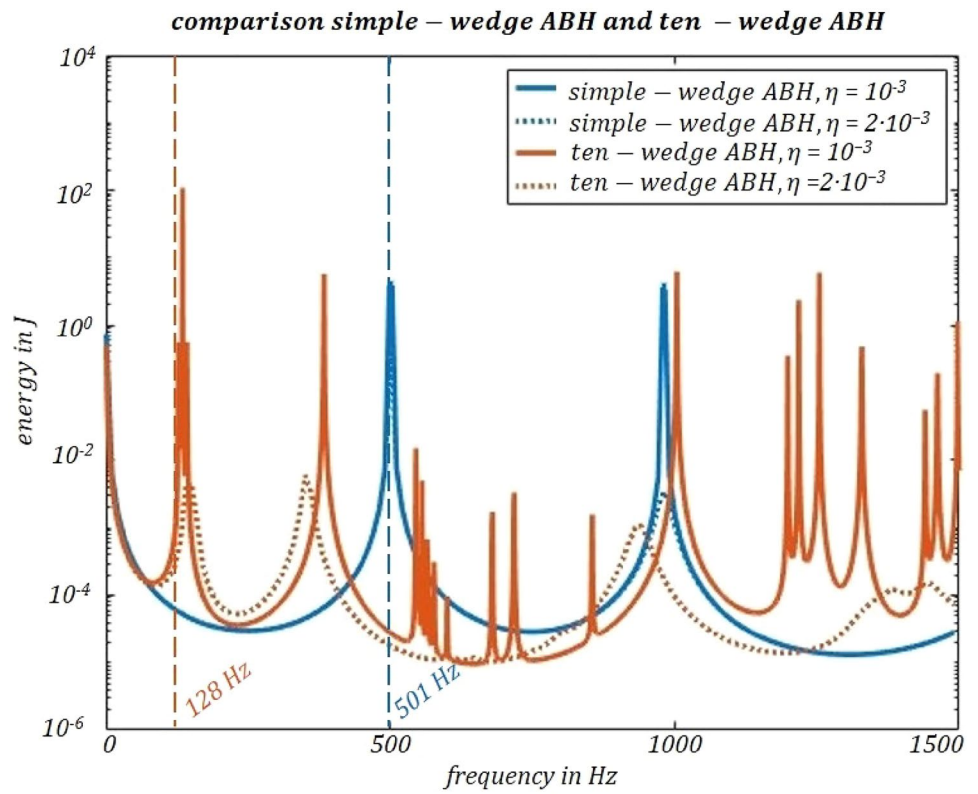
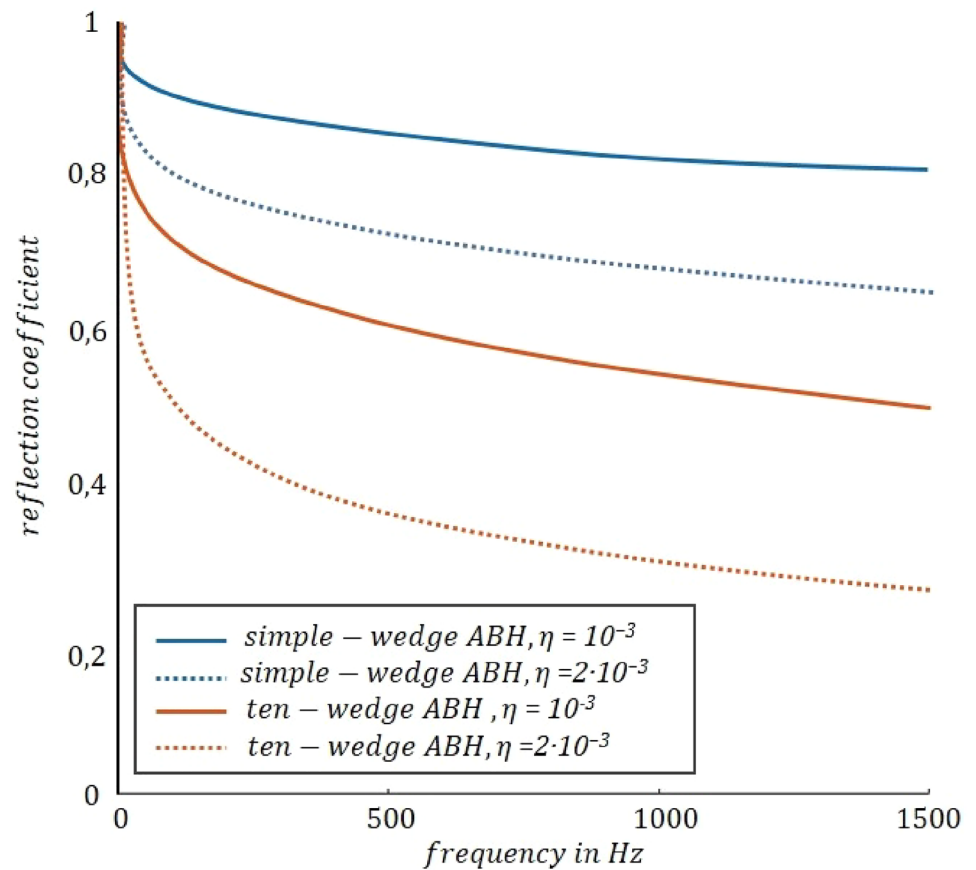


**Fig. 11** Reflection coefficient (Eq. (15)) for a simple-wedge ABH and ten-wedge ABH with  $l_{abh}=50$  mm for  $m=4$  with different loss-factors  $\eta$



increasing  $\eta$  from  $10^{-3}$  to  $2 \cdot 10^{-3}$ , the reflection coefficient of the ABH can be reduced significantly.

## Conclusion

- Tunability of multi-wedge ABH towards low-frequency in terms of cut-on frequency and reflections coefficient
- Analytical derivation of relative displacement of a wave travelling into the ABH and out of the ABH based on WKB-approximation with use case
- Comparison of performance to the simple wedge ABH

The analytical and theoretical approach to calculate and determine the reflection coefficient showed significant results. The comparison for a simple-wedge ABH stated, that an ABH with the exponent  $m=4$  in the power law curve results in much lower reflection coefficients than with an exponent on  $m=2$ . A lower reflection coefficient underlines a better working ABH, resulting in less induced energy reflected back into the host structure. The application of a damping layer can increase the ABH effect. Calculating the reflection coefficient with Eq. (15) and  $h_{tip} \ll 0,1$  mm leads mathematically to more exact results for a higher performing ABH than using Eq. (5) and  $h_{tip} \geq 0,1$  mm. Due to limitations in the production of the ABH, an  $h_{tip} \ll 0,1$  mm is very difficult to achieve in reality. The damping layer also absorbs the energy of the oscillating ABH. For the multi-wedge ABH an analytical derived reflection coefficient was stated. The ten-wedge ABH used for this paper theoretically resulted in much lower  $R_0$  values compared to a simple-wedge ABH in the selected frequency range.

The comparison of the cut-on frequency for a simple-wedge ABH with  $m=2$  and  $m=4$  showed that the exponent  $m=4$  lowers the cut-on frequency significantly. The cut-on frequency here sets a boundary at which frequency the ABH works effective and absorbs the induced vibrational energy. For practical applications ABH with an exponent of  $m=4$  result in benefits like less material to be used for manufacturing. Resulting in cheaper production costs.

With the WKB-approximation an approach to calculate the displacement of the ABH while a wave travelling into the ABH from  $x_{abh}$  to  $x_{tip}$  and out of it from  $x_{tip}$  to  $x_{abh}$  was performed successfully. It was evident that more accurate findings were obtained using a higher order approximation. The WKB-method could only perform successful in the higher frequency range. When a wave is travelling into the ABH then the relative displacement increases significantly. On the other hand the relative displacement decreases for a wave travelling out of the ABH. This underlines the effectiveness of the ABH.

**Acknowledgements** The authors gratefully acknowledge the financial support of this work within the project FFG Bridge #883698 from Micado Smart Engineering GmbH, IDM Energiesysteme GmbH and the Austrian Research Promotion Agency (Österreichische Forschungsförderungsgesellschaft mbH).

**Funding** Open access funding provided by FH Vorarlberg - University of Applied Sciences.

**Data availability** The datasets generated during and/or analyzed during the current study are available from the corresponding author on reasonable request.

**Open Access** This article is licensed under a Creative Commons Attribution 4.0 International License, which permits use, sharing, adaptation, distribution and reproduction in any medium or format, as long as you give appropriate credit to the original author(s) and the source, provide a link to the Creative Commons licence, and indicate if changes were made. The images or other third party material in this article are included in the article's Creative Commons licence, unless indicated otherwise in a credit line to the material. If material is not included in the article's Creative Commons licence and your intended use is not permitted by statutory regulation or exceeds the permitted use, you will need to obtain permission directly from the copyright holder. To view a copy of this licence, visit <http://creativecommons.org/licenses/by/4.0/>.

## References

1. Hartog JPD (1985) Mechanical Vibrations, Dover Publications, INC, New York
2. Altay O (2021) Vibration Mitigation Systems in Structural Engineering. CRC Press. <https://doi.org/10.1201/9781315122243>
3. J. Tang, K. Wang, Encyclopedia of vibration - hybrid control (2001) 649–658 <https://doi.org/10.1006/rwvb.2001.0196>
4. A. Pelat, F. Gautier, S. Conlon, F. Semperlotti, The acoustic black hole: A review of theory and applications, Journal of Sound and Vibration 476 Article 115316 (2020)
5. Mironov MA (1988) Propagation of a flexural wave in a plate whose thickness decreases smoothly to zero in a finite interval. Sov. Phys. Acoust. 34:318–319
6. V. Krylov, Acoustic black holes and their applications for vibration damping and sound absorption (2012) 933–944
7. Lee J, Jeon W (2017) Vibration damping using a spiral acoustic black hole 141:1437
8. Aklouche O, Pelat A, Maugeais S, Gautier F (2016) Scattering of flexural waves by a pit of quadratic profile inserted in an infinite thin plate. J Sound Vib 375:38–52. <https://doi.org/10.1016/j.jsv.2016.04.034>
9. M. Käfer, F. Dohnal, V. Goettgens, J. Stajkovic, M. Brunner, G. Leichtfried, Experimental verification of additively manufactured stacked multi-wedge acoustic black holes in beams for low frequency - in review, Mechanical Systems and Signal Processing (2023)
10. Krylov V, Tilman F (2004) Acoustic 'black holes' for flexural waves as effective vibration dampers. J Sound Vib 274:605–619
11. Zhao C, Prasad MG (2019) Acoustic black holes in structural design for vibration and noise control. Acoustics 1:220–247
12. Feurtado P, Conlon S, Semperlotti F (2014) Normalized wave number variation parameter for acoustic black hole design. J Acoust Soc Am 136:48–152
13. D. O'Boy, V. Krylov, V. Kralovic, Damping of flexural vibrations in rectangular plates using the acoustic black hole effect, J. Sound Vib. 329 (2010) 4672–4688

14. Zhao L (2016) Passive vibration control based on embedded acoustic black holes. *J Vib Acoust* 138(041002):605–619
15. D. Ross, E. Ungar, E. K. Jr., Damping of plate flexural vibrations by means of viscoelastic laminae, J.E. Ruzicka (Ed.), *Structural Damping* (1960) 49–87
16. Kravchun P (1991) Generation and methods of reduction of noise and vibration. Moscow University Press, Moscow (in Russian)
17. E. Ungar, Vibration isolation and damping, in: M.j. crocker (ed.), *handbook of acoustics, Handbook of Acoustics* (1998) 675–687 (Chapter 55)
18. K. Hook, J. Cheer, S. Daley, A parametric study and modal analysis of an acoustic black hole on a beam, *International Conference on Noise and Vibration Engineering (ISMA) 2018* (2018)
19. Krylov VV (2014) Acoustic black holes: recent developments in the theory and applications. *IEEE Trans Ultrason Ferroelectr Freq Control* 61:1296–1306
20. Huang W, Ji H, Qiu J, Cheng L (2018) Analysis of ray trajectories of flexural waves propagation over generalized acoustic black hole indentations. *J Sound Vib* 417:216–226
21. D. O'Boy, D. Bowyer, V. Krylov, Damping of flexural vibrations in thin plates using one and two dimensional acoustic black hole effect (2010)
22. H. Ji, W. Huang, J. Qiu, L. Cheng, Mechanics problems in application of acoustic black hole structures, *Adv Mech* 47 (2017)
23. A. Karlos, Wave propagation in non-uniform waveguide; doctoral thesis, University of Southampton Research Repository (2020)
24. Pierce AD (1970) Physical interpretation of the wkb or eikonal approximation for waves and vibrations in inhomogeneous beams and plates. *J Acoust Soc Am* 48(1B):275–284
25. Firouz-Abadi RD, Haddadpour H, Novinzadeh AB (2007) An asymptotic solution to transverse free vibrations of variable-section beams. *J Sound Vib* 304(3–5):530–540
26. Karlos A, Elliott SJ, Cheer J (2019) Higher-order wkb analysis of reflection from tapered elastic wedges. *J Sound Vib* 449:368–388
27. L. Cremer, M. Heckl, B. A. T. Petersson, *Structure-borne sound: Structural vibrations and sound radiation at audio frequencies* (2005)
28. Chakraverty S (2009) *Vibration of Plates*. CRC Press, Taylor and Francis Group, United States of America
29. Nielsen R, Sorokin S (2014) The wkb approximation for analysis of wave propagation in curved rods of slowly varying diameter. *Proc R Soc A* 470(2167):20130718–20130718

**Publisher's Note** Springer Nature remains neutral with regard to jurisdictional claims in published maps and institutional affiliations.